Vibrational Analysis of the $H_5O_2^+$ Infrared Spectrum Using Molecular and Driven Molecular Dynamics†

Martina Kaledin,* Alexey L. Kaledin, and Joel M. Bowman

Department of Chemistry and Cherry L. Emerson Center for Scientific Computing, Emory University, Atlanta, Georgia 30322

Received: August 5, 2005; In Final Form: September 19, 2005

Standard molecular and driven molecular dynamics are used to analyze prominent spectral features in the $H_5O_2^+$ infrared spectrum. In the driven method, the molecular Hamiltonian is augmented with a time-dependent term, $\vec{\mu} \cdot \vec{\varepsilon}_0 \sin(\omega t)$, where $\vec{\mu}$ is the dipole moment of $H_5O_2^+$, $\vec{\varepsilon}_0$ is the electric field, and ω is the frequency. The magnitude of the electric field determines whether the driving is mild (the harmonic limit) or strong (anharmonic motion and mode coupling). We analyze the spectrum in the wavenumber range from 600 to 1900 cm^{-1}, where recent experimental measurements are available for $H_5O_2^+$. On the basis of the simulations, we have assigned the broad feature around 1000 cm^{-1} to the proton transfer coupled with the torsion motion. Intense absorption near 1780 cm^{-1} is assigned to the H_2O monomer bend coupled with proton transfer.

1. Introduction

Proton transport is of great interest to science since it plays an important role in many chemical and biological processes. The nature and transport mechanism of a proton in aqueous solutions, and its spectroscopic signatures, has been the subject of extensive study for many years.[1−3] For example, the understanding of the migration of protons in water is essential to explain charge transport across cell membranes. Protons (H^+) and hydroxide ions (OH^-) exhibit abnormal mobility in aqueous solutions as compared to other ions, such as sodium (Na^+) and chlorine (Cl^-).[4] According to experiments and theory,[4−8] proton transfer in aqueous solutions occurs via a rearrangement of hydrogen bonds rather than migration of these ions in space.

To unravel the complex processes in biological systems, the elementary species involved in proton mobility, $H_5O_2^+$ and $H_3O_2^-$, have been studied extensively both theoretically and experimentally.[8−33] However, only partial spectra of $H_5O_2^+$ have been recorded in the gas phase. In particular, the vibrational frequencies corresponding to the proton transfer are still not well-understood because the potential energy surface (PES) of $H_5O_2^+$ is very flat in the vicinity of its minimum,[15] and motion of the proton between the two water monomers is expected to be extremely floppy and anharmonic.

Two groups[9,10] recently measured gas phase infrared multiple photon dissociation (IRMPD) spectra for the proton-bound dimer in the low energy range (620−1900 cm^{-1}) using high power infrared (IR) free-electron lasers. Predissociation spectra of the $H_5O_2^+ \cdot RG_n$ (RG = Ar, Ne) cluster ions were reported by Johnson's group.[34−36] IRMPD spectra identify relatively broad bands throughout the 620−1900 cm^{-1} range. Although there are four main features in both spectra,[9,10] they are clearly different in both positions and intensities. However, the two spectra were measured at different temperatures (100 and 300 K); therefore, broadening of the features would be expected rather than a frequency shift. A possible explanation for the disagreement would be that at high temperatures, there are other $H_5O_2^+$ isomers accessible.[9]

On the basis of several theoretical calculations,[9,26] different assignments of the spectral features were attributed to the bridging proton stretch, intramolecular bends, and various combination bands. The accuracy of assignment of spectra relies mainly on the quality of the PES and the treatment of the vibrational dynamics. The anharmonicity of the PES, the strong mode coupling, and the multidimensional nature of the proton transfer make the evaluation of the vibrational frequencies of $H_5O_2^+$ a difficult task. Direct ab initio molecular dynamics (MD) simulations of proton transfer in $H_5O_2^+$ [31] indicated that the characteristic frequencies of proton motion are strongly temperature-dependent and coupled to other modes. The motion corresponding to a given peak was identified from the spectrum of partial density of states. The partial density of states was obtained by Fourier transform of averaged velocity−momentum correlation function over a reduced subset of the modes of $H_5O_2^+$. However, computing the IR or Raman vibrational spectrum would require evaluation of a dipole correlation function; and therefore, the assignment of spectra based on partial density of states is inconclusive.

Motivated by uncertainties in experimental results, we present classical MD and driven MD (DMD) simulations of the temperature dependence of spectra of $H_5O_2^+$ in the range from 600 to 1900 cm^{-1} and the OH stretching range from 3700 to 3900 cm^{-1}, as well. Recently, Huang et al. has developed global full-dimensional PES and dipole surfaces for $H_5O_2^+$.[27] This potential surface was used in recent quantum diffusion Monte Carlo and variational calculations of vibrational energies of the ground state and OH stretch fundamentals.[28,36] We use the global PES and dipole surfaces to calculate the IR spectra of $H_5O_2^+$ at various temperatures and assign the spectral features using the DMD method.[37−39] This method follows from a basic characteristic of normal modes, which means that a classical system executing small amplitude motion about a minimum can be driven resonantly at the normal-mode frequency. The system will respond to a given mild driving at resonant frequency by

† Part of the special issue "Jürgen Troe Festschrift".

* To whom correspondence should be addressed. E-mail: mkaledi@emory.edu. Present address: Department of Chemistry and Biochemistry, Kennesaw State University, Kennesaw, GA 30144.

10.1021/jp054374w CCC: $33.50
Published on Web 10/29/2005

executing the corresponding normal-mode vibration. On the other hand, applying the strong driving force yields anharmonic motion. The analysis of the atomic motion stimulated by driving at resonant frequencies is used here to assign the spectral features.

The paper is organized as follows. Section 2 reviews the details of the DMD method and calculation of the thermal spectra. In section 3, we present the thermal spectra of $H_5O_2^+$, compare them to the relevant experimental measurements, and discuss the assignment of the spectral features. Finally, a summary and conclusions are given in section 4.

2. Theoretical Methods

In this section, we give details of the calculation of the temperature dependence of IR spectra of $H_5O_2^+$ using classical MD simulations. The interaction potential function and dipole moment surface that we use in MD simulations were developed in our group.[27] Full-dimensional ab initio PES and dipole moment surfaces were calculated at CCSD(T)/aug-cc-pVTZ and MP2/aug-cc-pVTZ computational levels, respectively. Ab initio data were fitted very accurately in terms of all internuclear distances using least-squares procedures, however, with a fitting basis that satisfies permutational symmetry of identical atoms. The PES can describe internal floppy motions, including the H atom exchanges, monomer inversions, and monomer torsions, and it dissociates correctly to $H_2O + H_3O^+$ with $D_e = 11924$ cm^{-1}.

2.1. Calculation of Thermal Spectra. The classical MD simulation of IR spectra[40] is well-known and routinely used nowadays, especially in applications to large molecular systems. The expression for the IR spectrum of a system at temperature $T = 1/k_B\beta$ (k_B is Boltzmann constant) is

$$I_{\mu\mu}(\omega) = \frac{\mathscr{R}e}{\pi}\int_0^\infty \mathrm{d}t\, e^{i\omega t}\langle \vec{\mu}_0 \cdot \vec{\mu}_t \rangle_\beta \tag{1}$$

where the dipole−dipole correlation function is a Boltzmann average

$$\langle \vec{\mu}_0 \cdot \vec{\mu}_t \rangle_\beta = \frac{tr[e^{-\beta H}\,\vec{\mu}_0 \cdot \vec{\mu}_t]}{tr[e^{-\beta H}]} \tag{2}$$

where H is the full classical Hamiltonian. Equation 2 can be recast as a ratio of two integrals

$$\langle \vec{\mu}_0 \cdot \vec{\mu}_t \rangle_\beta = \frac{\int \mathrm{d}\mathbf{p}_0 \int \mathrm{d}\mathbf{q}_0\, e^{-\beta H(\mathbf{p}_0,\mathbf{q}_0)}\vec{\mu}_0 \cdot \vec{\mu}_t}{\int \mathrm{d}\mathbf{p}_0 \int \mathrm{d}\mathbf{q}_0\, e^{-\beta H(\mathbf{p}_0,\mathbf{q}_0)}} \tag{3}$$

where $\vec{\mu}_0 \cdot \vec{\mu}_t$ is the sampled quantity weighted by $e^{-\beta H(\mathbf{p}_0,\mathbf{q}_0)}$. The dipole depends on the initial phase point $(\mathbf{p}_0,\mathbf{q}_0)$ through the time propagation of the coordinate, $\vec{\mu}_t = \vec{\mu}\,[\mathbf{q}_t(\mathbf{p}_0,\mathbf{q}_0)]$. At zero temperature, the system can be described as oscillating harmonically around the global minimum. With increasing temperatures, a molecule can explore wider regions of its configurational space. A canonical distribution of molecular configurations is generated using the standard Metropolis "random walk" algorithm.[41] The Metropolis sampling method consists of generating a set of molecular configurations by random displacements of the particles. A Monte Carlo move is defined by the following equations

$$\mathbf{q}_0^{\,k+1} = \mathbf{q}_0^k + \left(\xi_1 - \frac{1}{2}\right)\Delta\mathbf{q} \tag{4}$$

$$\mathbf{p}_0^{\,k+1} = \mathbf{p}_0^k + \left(\xi_2 - \frac{1}{2}\right)\Delta\mathbf{p}$$

where ξ_i is a random Cartesian vector sampled from a uniform distribution on the interval (0,1) and $\Delta\mathbf{q}$, $\Delta\mathbf{p}$ are the sizes of the attempted moves in the respective coordinates. A new configuration is always accepted, if the change in total energy ΔE associated with this move is negative, or else it is accepted with a probability of $\exp(-\Delta E/k_BT)$. $\Delta\mathbf{q}$, $\Delta\mathbf{p}$ are adjusted such that ~50% of the attempted moves are accepted. The standard strategy is to start with arbitrary coordinates and momenta (we choose the equilibrium structure and zero momenta) and then equilibrate the sample at a particular temperature. Typically, thermal equilibrium is reached after 10^4-10^5 steps. Then, ensemble averages are obtained from MD simulation runs as

$$\langle \vec{\mu}_0 \cdot \vec{\mu}_t \rangle_\beta = \frac{1}{K}\sum_{k=1}^{K} \vec{\mu}(\mathbf{q}_0^k) \cdot \vec{\mu}(\mathbf{q}_t^k) \tag{5}$$

where K is the number of chosen phase space points—initial conditions for classical trajectories. To achieve statistical independence, every 2000th accepted configuration is included in the process of averaging. The spectrum $I_{\mu\mu}$ can then be calculated by Fourier transform of eq 5. To improve the convergence of eq 5 with the number of trajectories, we employ a time averaging procedure to smooth the dipole−dipole correlation function[42]

$$I_{\mu\mu}(\omega) = \frac{s_\beta}{2\pi t K}\sum_{k=1}^{K}\sum_{\alpha=x,y,z} \left|\int_0^t \mathrm{d}\tau e^{i\omega\tau}\,\mu^\alpha(\mathbf{q}_\tau^k)\right|^2 \tag{6}$$

where s_β is a quantum symmetrization factor[40] defined as $s_\beta = \beta\hbar\omega/[1 - \exp(-\beta\hbar\omega)]$. The time integral in the square brackets is evaluated by Fourier transform. We run 100 trajectories for temperatures 100 and 300 K relevant to the experimental measurements.

2.2. Assignment of Spectra. Classical MD simulation yields IR spectra that can be directly compared to the experimental measurements. These IR spectra can often reproduce the observed experimental patterns; however, one often faces difficulties with the assignment of vibrational bands. This is especially problematic for $T > 0$ simulations where complex features of the spectra cannot be assigned by the double harmonic approximation. Here, we propose a classical method of assignment of the spectral features using DMD. This method was originally developed to calculate the normal-mode frequencies and normal-mode vectors of large molecules.[37−39] DMD employs an external, driving term that can be used to scan the spectrum and to determine resonant absorptions. The most attractive feature of DMD, and advantage over Hessian techniques, is the ability to include anharmonic effects directly into the driving scheme. Mild driving (small driving force) is used to extract the harmonic normal modes; harder driving can be used to study anharmonic effects.[38,39]

The Hamiltonian of a molecular system in DMD simulation consists of the molecular Hamiltonian, H_0, and a driving term, $U(\mathbf{q}_t, t; \omega)$

$$H(\mathbf{p}_t,\mathbf{q}_t,t) = H(\mathbf{p}_t,\mathbf{q}_t) + U(\mathbf{q}_t,t;\omega) \tag{7}$$

where ω is the driving frequency. In our previous work,[37,38] the driving force was applied to all interatomic distances in order to excite only vibrations of a molecule. A particular vibrational mode directly absorbs IR electromagnetic radiation, if the

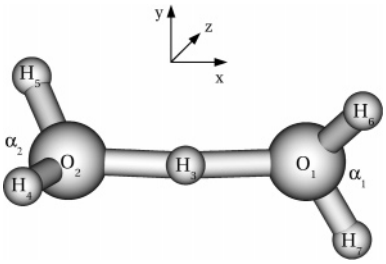

Figure 1. Coordinate system of $H_5O_2^+$. α is a H−O−H angle.

vibrational motion associated with that mode produces a change in the dipole moment of the molecule. Thus, to obtain the spectrum, we use a dipole-driving term[39]

$$U(\mathbf{q}_t,t;\omega) = \vec{\mu}(\mathbf{q}_t)\cdot\vec{\varepsilon}_0\sin(\omega t) \tag{8}$$

where $\vec{\varepsilon}_0$ is the electric field vector and $\vec{\mu}(\mathbf{q}_t)$ is the electric dipole of the molecule, whose first derivative with respect to the Cartesian coordinates enters the equations of motion.

To identify the resonant frequencies, we monitor the average total internal energy of the molecule after time t

$$\langle E\rangle_t = \frac{1}{t}\int_0^t \mathrm{d}\tau H_0(\mathbf{p}_\tau,\mathbf{q}_\tau) \tag{9}$$

At nonresonant frequencies, the absorbed energy is small and oscillatory with time, while on resonance it increases rapidly with time.

The frequency range of interest is scanned with a uniform step $\Delta\omega$. For each frequency, the trajectory is propagated for several picoseconds. The system can be initially at the equilibrium structure with zero momenta ($\mathbf{q} = \mathbf{q}_e$, $\mathbf{p} = 0$). In DMD simulations carried out at the thermally excited structures, configurations are selected from the Boltzmann distribution at temperature T using the technique described in the previous section. During the simulation, the absorption energy (eq 9) is monitored to identify a resonant frequency. At resonant frequencies, the atomic motion is analyzed along the trajectory and the spectral features are assigned. The coordinate system of the C_2 point group equilibrium structure is shown in Figure 1. The X-axis is coincident with the OO-axis, and the C_2 rotation axis is chosen to be the Z-axis.

3. Results

3.1. MD Simulations. The MD simulations were performed at two temperatures, 100 and 300 K. The initial conditions of trajectories were sampled using the Metropolis algorithm discussed in section 2.1. The MD time step was 0.25 fs, and trajectories were propagated for about 8 ps resulting in a 4 cm^{-1} resolution for the IR spectrum. Under these conditions, the error in the total energy was confined to less than 0.2% of the total energy for all trajectories. For each temperature, the spectrum was calculated from 100 trajectories. We tested the convergence of the spectrum with the number of trajectories by running another 100 trajectories with different initial conditions. The shapes of the spectra from the two sets of simulations were very similar. The thermally averaged dipole−dipole correlation function was calculated according to eq 5.

The resulting classical MD spectra and the quantum harmonic spectrum are shown in Figure 2. There is strong activity in the range from 600 to 1900 cm^{-1}. At 100 K, there are four main bands near 860, 1000, 1480, and 1780 cm^{-1}. The spectrum is qualitatively consistent with the IRMPD experiment of Asmis et al. in which three of the five main bands are identified around

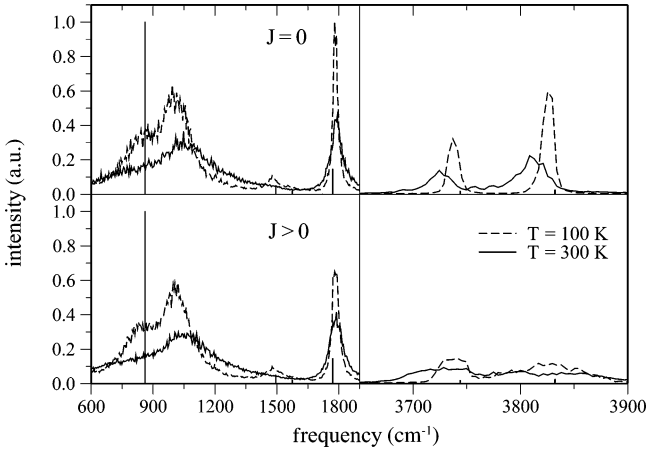

Figure 2. Results of MD simulations for the IR spectra of $H_5O_2^+$ at 100 (dashed line) and 300 K (solid line). Upper panels show results from $J = 0$ simulations, and lower panels show $J > 0$ simulations. All spectra have been normalized so that the largest peak value for $J = 0$ is equal to 1. The quantum harmonic IR spectrum is shown as sticks. The presented spectra are averaged over 100 trajectories. Each trajectory was propagated for 8 ps.

900, 1100, and 1750 cm^{-1} and labeled B, C, and E, respectively (cf. Figure 7 of ref 10). The absence of a strong feature around 1300 cm^{-1} in the theoretical spectrum is the main discrepancy with the IRMPD experiment. Rare gas predissociation measurements[34−36] reveal a dominant sharp feature around 1050 cm^{-1} and a weaker feature just below 1800 cm^{-1}. Interestingly, when Ne was used as the rare gas messenger instead of Ar, a weak activity in the form of broad peaks between 1300 and 1500 cm^{-1} was detected.[36]

The effect of temperature on the simulated spectra is clearly seen. At higher temperature, $T = 300$ K, $H_5O_2^+$ becomes more flexible and significantly distorted from its minimum energy configuration. Accordingly, the widths of the absorptions in the averaged IR spectra increase and peaks shift, leaving only two main bands near 1000 and 1780 cm^{-1}. Similar patterns were observed in ab initio MD simulations.[25,26] Although the temperature is not well-defined in the predissociation experiments, it is plausible that the Ne-bound complex is captured at lower temperature than the Ar-bound complex due to both the lighter mass of the rare gas atom and the weaker interaction with $H_5O_2^+$. The disappearance of the peak at 1480 cm^{-1} in the theoretical spectrum with increasing temperature is consistent with the Ar predissociation experiments. In the OH stretch part of the spectrum, a detailed picture of the region above 3500 cm^{-1} shows two bands that are broadened and shifted with increasing temperature, not dissimilar to the rare gas messenger pattern of Ne vs Ar.[36]

We present results for both $J = 0$ and $J > 0$ simulations. Total angular momenta (J values) calculated from 100 trajectories are up to 40 and 65 for 100 and 300 K, respectively. $H_5O_2^+$ is a prolate symmetric top with the rotation constants $A = 5.813$ cm^{-1}, $B = 0.290$ cm^{-1}, and $C = 0.288$ cm^{-1} at the equilibrium structure depicted in Figure 1. Similar values for the rotation constants were obtained previously at MP2 and DFT computational levels.[43] Rotation causes broadening of the vibrational lines, especially in the regions of 1800 cm^{-1} and OH stretching frequencies at 3800 cm^{-1}.

3.2. DMD Simulations at the Equilibrium $H_5O_2^+$. It will be useful to analyze the motion of $H_5O_2^+$ in DMD calculations in terms of the standard normal modes. To do so, we use a procedure that is commonly used in standard MD simulations, e.g., biomolecules.[44] The procedure is to generate a time series

TABLE 1: Diagonal Elements of the Overlap Matrix[a]

ω (cm^{-1})	$\|\varepsilon_x\| = 1.0 \times 10^{-5}$ (a.u.)[b]	$\|\varepsilon_x\| = 1.0 \times 10^{-4}$ (a.u.)[c]
170	0.987	0.848
339	0.995	0.843
471	0.974	0.852
532	0.954	0.741
554	0.984	0.861
630	0.995	0.404
861	0.998	0.700
1494	0.925	0.645
1574	0.990	0.784
1720	0.991	0.519
1770	0.940	0.841
3744	0.691	0.621
3750	0.182	0.207
3832	0.491	0.367
3832	0.385	0.273

[a] Average weights represent the overlap between the normal-mode vectors from standard NMA and DMD calculations. [b] The calculations were performed with double harmonic approximation. [c] The calculations were performed with full potential.

of the projection of the MD trajectory positions into a mode of interest. One procedure for comparing normal modes from different simulations is by computing an inner product of the two modes.[44] First, we calibrate the DMD method for $H_5O_2^+$ in the harmonic limit. We performed a standard normal-mode analysis (NMA) by diagonalizing the Hessian matrix at the equilibrium structure and obtained the 15 normal-mode frequencies ω_j and the corresponding normal-mode vectors u_j. Next, we carried out DMD simulations with the harmonic potential to eliminate anharmonicities, $V = (1/2)\Delta\mathbf{q}^T\mathbf{K}\Delta\mathbf{q}$, where $\mathbf{K}$ is the Hessian. The molecule is initially at rest at the equilibrium structure, and the driving force at frequency ω_j is weak, $|\vec{\varepsilon}_0| = 1.0 \times 10^{-5}$ a.u. (0.86 cm^{-1}/Debye) to ensure that molecule responded by harmonic motion. (Note that NMA is harmonic approximation, and for the purpose of the calibration of DMD, we want to keep atomic motion harmonic.) After a significant amount of energy is absorbed by the molecule, atomic displacements are evaluated. The normalized mass-scaled displacements at time t were obtained from the $3N$ Cartesian coordinates as follows,

$$\Delta x_i(t) = \frac{m_i^{1/2}(q_{ti} - q_{ei})}{[\sum_{i=1}^{3N} m_i(q_{ti} - q_{ei})^2]^{1/2}} \tag{10}$$

To quantify how given DMD displacements compare with the normal-mode vectors, the overlap between the two sets along the trajectory is evaluated

$$O_j(t) = \Delta\mathbf{x}(t) \cdot \mathbf{u}_j = \sum_{i=1}^{3N} \Delta x_i(t) u_{ij} \tag{11}$$

where $\mathbf{u}_j$ is the j-th normal-mode vector. The overlap will be 1.0 if the two sets of modes are identical and 0.0 if they are orthogonal. The contribution of each normal mode to the trajectory propagated at any frequency can be defined as an average weight, $w_j = 1/(N_t - 1)\sum_{l=1}^{N_t} O_j^2(t_l)$, where N_t is the number of recorded time frames. Table 1 shows the results of the DMD simulations with the electric field oriented along the X-axis. Similar results were obtained for Y- and Z-components of the electric field. The weights are close to 1 for almost all frequencies. Dipole driving for IR inactive modes could be problematic. These modes do not absorb a significant amount

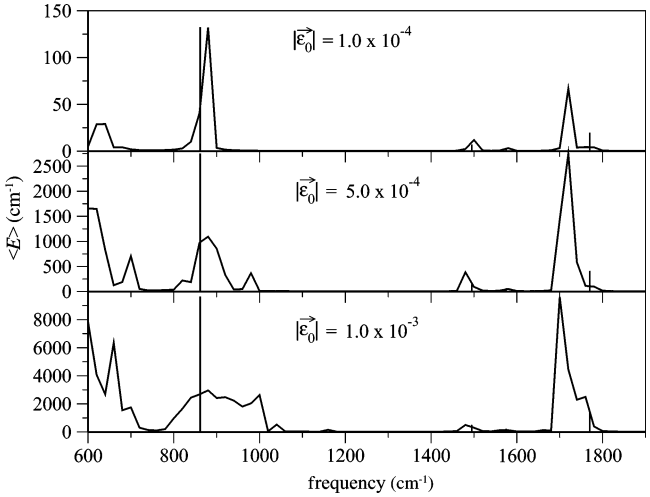

Figure 3. Results of DMD ($J = 0$) simulations at the equilibrium structure of $H_5O_2^+$. The spectrum was scanned in the region from 600 to 1900 cm^{-1} with a 20 cm^{-1} step. For each frequency, a trajectory was propagated for 8 ps. The quantum harmonic IR intensities are shown as sticks for comparison (scaled to the maximum of the driven spectrum for each field strength). The averaged absorbed energy $\langle E \rangle$ is a sum of three trajectories corresponding to the electric field oriented along X-, Y-, and Z-axes.

of energy and, therefore, are difficult to resolve. For example, IR activity of two adjacent frequencies 3744 and 3750 cm^{-1} separated by only 6 cm^{-1} is much less than for the other frequencies. In such a case, the overlap between the Hessian normal-mode vectors and DMD displacements is not perfect. The values of 3744 and 3750 cm^{-1} are combinations of 3744 and 3750 cm^{-1} frequencies with weights 0.691 and 0.200 and 0.780 and 0.182, respectively. Also, two overlapping frequencies at 3832 cm^{-1} cannot be resolved by dipole driving, and their overlap is only 0.385 and 0.491.

We gradually increased the electric field $|\vec{\varepsilon}_0| = (1.0, 5.0,$ and $10.0) \times 10^{-4}$ a.u. and performed DMD simulations with full potential. In these simulations, anharmonic effects are implicitly included and can be analyzed. From the atomic positions, we again calculated the overlap and average weights for resonant frequencies. The spectrum was scanned in the range from 600 to 1900 cm^{-1} with a 20 cm^{-1} step in order to determine the resonant frequencies. For each frequency, we propagated three ($J = 0$) trajectories for a time of 8 ps with the electric field oriented along X-, Y-, and Z-axes, respectively. This helps us to understand the symmetry-related absorptions. The average absorbed energy $\langle E \rangle$ as a function of frequency is shown in Figure 3. $\langle E \rangle$ increases rapidly with increasing the intensity of the electric field. DMD simulation with electric field $|\vec{\varepsilon}_0| = 1.0 \times 10^{-4}$ a.u. reproduces the harmonic spectrum quite well. The positions of the maximum energy peaks still agree very well with the normal-mode frequencies indicated by the sticks in the spectrum. However, atomic motion starts to show anharmonicity, and the overlap between the Hessian normal modes and DMD displacements decreases. (Compare average weights from this calculation and the benchmark calculations at $|\vec{\varepsilon}_0| = 1.0 \times 10^{-5}$ a.u. in Table 1.) Possible mixing between the modes is reflected in the overlaps. For example, the absorbing mode at 1720 cm^{-1} is mixed with the O···H$^+$···O proton transfer asymmetric stretch at 861 cm^{-1}. According to the quantum double harmonic calculation, the intensity of IR absorption is very low for the symmetric H_2O bend at 1720 cm^{-1}. However, this mode couples with the asymmetric O···H$^+$···O stretching mode at 861 cm^{-1} what appears to be a Fermi-like 2:1 resonance. Thus, because 861 cm^{-1} is IR active, the bend mode

TABLE 2: Overlap Matrix Showing Average Weights of the Overlap of the Driven Frequencies ω_{DMD} with the Normal-Mode ω_{NMA}[a]

ω_{NMA} / ω_{DMD}	axis	170	339	471	532	554	630	861	1494	1574	1720	1770
620	*X*	0.127	0.177	0.115	0.078	0.176	0.184	0.055	0.013	0.019	0.014	0.008
	Y	0.106	0.220	0.128	0.061	0.136	0.244	0.058	0.017	0.005	0.018	0.004
	Z	0.158	0.168	0.108	0.050	0.222	0.107	0.059	0.010	0.024	0.019	0.013
860	*X*	0.126	0.148	0.081	0.018	0.206	0.101	0.143	0.013	0.033	0.079	0.011
	Y	0.002	0.191	0.006	0.005	0.043	0.125	0.539	0.023	0.000	0.062	0.004
	Z	0.331	0.146	0.075	0.038	0.131	0.068	0.106	0.008	0.030	0.029	0.009
980	*X*	0.044	0.445	0.034	0.032	0.077	0.172	0.151	0.013	0.006	0.009	0.016
	Y	0.017	0.490	0.014	0.028	0.062	0.183	0.172	0.004	0.001	0.015	0.013
	Z	0.259	0.344	0.045	0.091	0.053	0.140	0.052	0.007	0.003	0.004	0.002
1580	*X*	0.168	0.020	0.002	0.002	0.011	0.037	0.065	0.001	0.646	0.045	0.003
	Y	0.018	0.081	0.010	0.008	0.008	0.040	0.106	0.106	0.569	0.004	0.049
	Z	0.629	0.022	0.022	0.023	0.001	0.010	0.024	0.030	0.211	0.026	0.002
1720	*X*	0.019	0.097	0.008	0.003	0.049	0.109	0.322	0.007	0.007	0.371	0.008
	Y	0.003	0.059	0.005	0.004	0.003	0.027	0.375	0.014	0.002	0.226	0.281
	Z	0.303	0.041	0.028	0.018	0.043	0.038	0.051	0.007	0.037	0.130	0.018
1780	*X*	0.003	0.023	0.003	0.001	0.013	0.043	0.174	0.001	0.015	0.206	0.518
	Y	0.005	0.046	0.004	0.004	0.003	0.024	0.048	0.009	0.001	0.002	0.850
	Z	0.518	0.013	0.014	0.014	0.000	0.005	0.037	0.003	0.004	0.085	0.307

[a] A trajectory was run up to 8 ps with a 0.25 fs time step for each driven frequency ω_{DMD}. The electric field $|\vec{\varepsilon}_0| = 5.0 \times 10^{-4}$ a.u. was oriented along the *X*-, *Y*-, and *Z*-axes, respectively.

at 1720 cm^{-1} becomes IR active as well through the coupling. The symmetric O···H^+···O stretch at 630 cm^{-1} is IR inactive in the double harmonic approximation; however, the DMD simulation shows significant absorption of energy near 630 cm^{-1}.

By increasing the electric field, $|\vec{\varepsilon}_0| = 5.0 \times 10^{-4}$ a.u., the molecule absorbs a significant amount of energy (Figure 3). At some point, the absorbed energy exceeds the harmonic limit. The shape of the spectrum becomes complicated due to the coupling between the modes, and atomic motion is perturbed by anharmonicity. Anharmonicity gives rise to the peaks at around 980 cm^{-1}. This spectral feature near 1000 cm^{-1} has been found in MD simulations at 100 and 300 K (Figure 2). Analyzing the atomic motion at this frequency using DMD simulation leads us to observe similarities with the atomic motion at 339 and 861 cm^{-1} (see Table 2), corresponding to the wagging motion and the proton transfer. Table 2 summarizes the overlap of the DMD displacements with the normal-mode vectors. DMD simulations were run for resonant frequencies (maximum peaks) shown in Figure 3 with the electric field oriented along the *X*-, *Y*-, and *Z*-axes. The results of simulation show that the atomic motion acquires significant torsion character almost at all resonant frequencies. On the basis of the DMD simulation, we conclude that both spectral features at 860 and 1000 cm^{-1} in the MD simulations correspond to the proton transfer in the presence of the torsion motion. The results of DMD simulations in MPEG format can be found on the website http://www.chemistry.emory.edu/faculty/bowman/news/index.html.

A further increase of the electric field, $|\vec{\varepsilon}_0| = 1.0 \times 10^{-3}$ a.u., leads to an extremely large absorption of energy by the molecule. The most active frequencies are 630 and 1720 cm^{-1}, and the spectral features between 800 and 1000 cm^{-1} are significantly broadened. At 860 and 980 cm^{-1}, DMD displacements overlap the best (about 10−20%) with 170, 339, 554, and 861 cm^{-1} normal-mode vectors associated with torsion, rocking, wagging, and proton transfer motion, respectively. In this simulation, the maximum absorbed energy reaches 10000 cm^{-1} and $H_5O_2^+$ eventually dissociates into $H_3O^+ + H_2O$.

3.3. DMD Simulations at the Thermally Excited Structure. We also performed driving at thermally excited configurations of $H_5O_2^+$ used for computing the MD spectrum. The $H_5O_2^+$ molecule was initially at the configurations corresponding to 100 K. We performed classical MD and DMD simulations at exactly the same starting configurations $(\mathbf{q}_0^k, \mathbf{p}_0^k)$ selected from the Boltzmann distribution by the Metropolis sampling. Because of the large computational cost of the DMD simulation (which involves running a set of trajectories for each frequency), we have chosen 11 out of 100 configurations used in MD simulations discussed in section 3.1. Each trajectory was propagated for 8 ps.

For resonant frequencies, we calculated trajectory statistics of the structural parameters at temperature $T = 100$ K. Various bond lengths and angles were evaluated along the trajectory. These quantities from the 11 trajectories were averaged at each time frame $\langle x(t_l) \rangle$. Also, the trajectory time average and the variance of the trajectory average $\bar{x}$ were evaluated, as follows,

$$\sigma^2 = \frac{1}{N_t - 1} \sum_{l=1}^{N_t} [\bar{x} - \langle x(t_l) \rangle]^2 \qquad (12)$$

where N_t is the number of recorded time frames. The difference between the trajectory statistics for MD and DMD simulations facilitates assignment of the spectral features. Here, we focus on the spectral absorption at 1780 cm^{-1}. Figure 4 is a result of classical MD and DMD simulations driven at 1780 cm^{-1} frequency. We monitored the H_2O monomer angle α, the O−O distance, and the position of the proton with respect to the center of mass of the O−O bond along the trajectory. The results of MD simulation demonstrate that the time-dependent quantities fluctuate about their equilibrium values with a small amplitude, while in DMD simulations the amplitudes are much larger. The 1780 cm^{-1} absorption can thus be assigned to a H_2O monomer bend coupled with proton transfer.

For resonant frequency at 1780 cm^{-1}, we also examine the variances of the average structural parameters, σ^2, as a function of field strength, $\vec{\varepsilon}_0$. Figure 5 summarizes the variances of internuclear distances and bond angle α. The O−H distance is

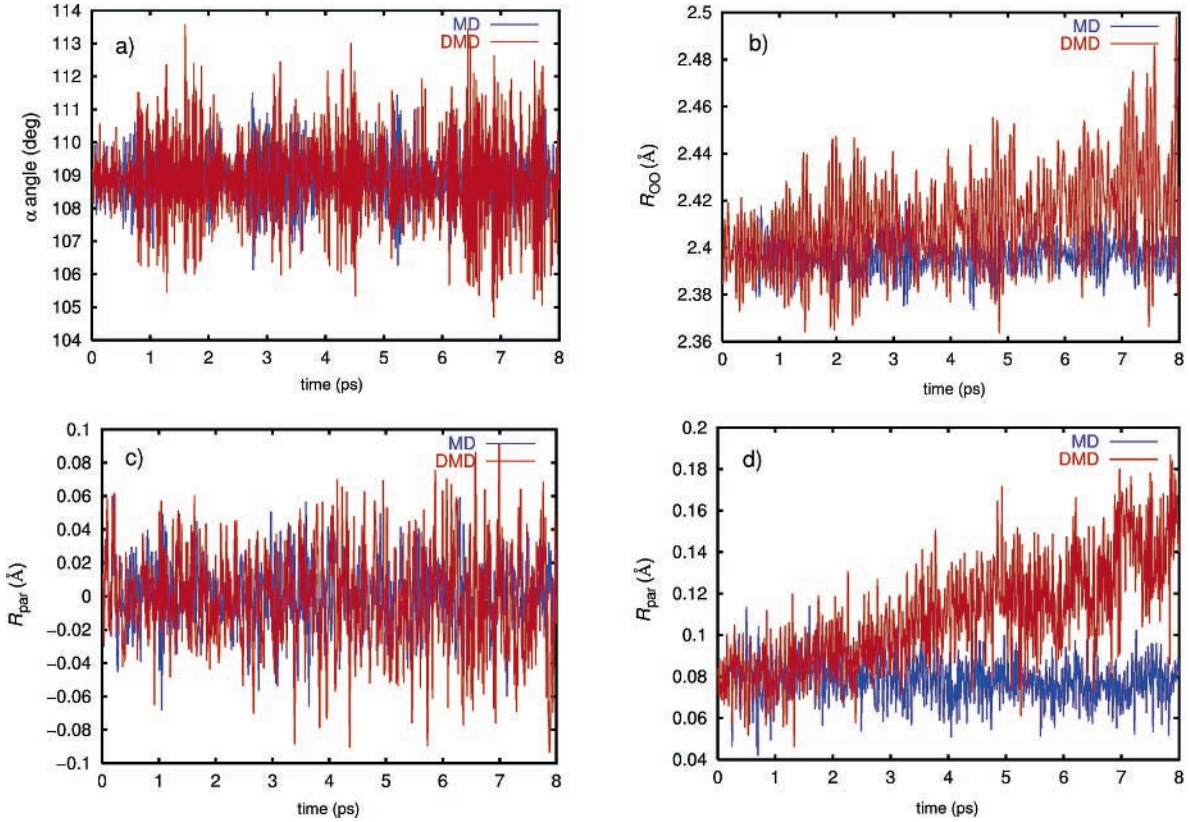

Figure 4. Results of MD simulations (in blue) and DMD driving (in red) at 1780 cm^{-1} frequency. Time-dependent sample averages of (a) H−O−H bond angle of water monomer, (b) O−O interatomic distance, (c) $O-H^+-O$ parallel component, and (d) $O-H^+-O$ perpendicular component of the distance from the center of mass of the O−O bond.

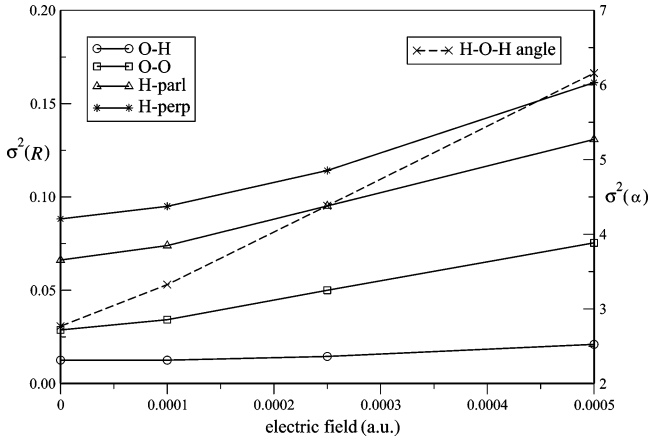

Figure 5. Variance of the average values as a function of the field strength for 1780 cm^{-1} frequency. Left *Y*-axis and solid lines refer to the variance of the distance (in $Å^2$), while right *Y*-axis and dashed lines refer to the variance of the H−O−H angle.

invariant to the increase of the electric field. The H−O−H angle and O−O and $O-H^+-O$ distances increase rapidly with the electric field, which means that the spectral feature at 1780 cm^{-1} consists of the H−O−H bending coupled with proton transfer.

The analysis shown in sections 3.2 and 3.3 leads to assignment of the IR spectrum of $H_5O_2^+$. Driving at thermally excited structures shows a lot of anharmonic motion along a trajectory. Therefore, we consider the proposed method of projection of the trajectory onto the normal modes as more suitable for the assignment of bands. However, both methods provide useful information about the atomic motion at resonant frequencies.

4. Summary and Conclusions

Despite the small size of $H_5O_2^+$, accurate characterization of its IR spectrum has been a major challenge due to a large number of strongly coupled degrees of freedom and the very floppy nature of the system. A reasonable simulation of IR spectra of system like this requires accurate PES and dipole moment function in order to describe anharmonic vibrations of the shared proton and rotations of the water monomers. In this work, we calculated the IR spectrum of $H_5O_2^+$ for temperatures 100 and 300 K using Monte Carlo MD simulations. The calculations of the spectra were based on the full dimensional PES and dipole surfaces.[27] Simulated IR spectra reproduce the observed IR patterns. Spectra at higher temperatures show peak shifts and broadening of the lines.

The present study provides a new DMD method regarding the assignment of the IR spectrum. Applying the weak external force to the molecule initiates molecular vibrations that are comparable to the normal-mode vibrations, while a strong external force can evoke anharmonic motions due to the mode coupling. Analysis of the molecular motion along the trajectory generated by DMD simulation leads to the assignment of the spectral features. Analyzing the classical and DMD trajectories shows that at higher temperatures torsional motion of molecules is involved. The broad feature between 800 and 1200 cm^{-1} predicted in MD simulations is assigned to proton transfer coupled with torsion motion. Strong absorption at 1780 cm^{-1} was assigned to H_2O bend and proton transfer.

Although the method of assignment of IR bands proposed in this work is based on a classical description of atomic motion and quantum effects were neglected, it can be a useful tool for interpretation of vibrational spectra. Simulated IR spectra may serve in the future as a guideline for experimental researchers

where to look for spectral features. For larger molecular systems, for example, $H_7O_3^+$ and $H_9O_4^+$, calculation of the PES and dipole surfaces is not feasible.

The DMD method combined with electronic structure theories (DFT, MP2, etc.) can provide a full dimensional treatment of the problem. The gradient of potential and dipole derivatives, essential for the evaluation of the driven term in equations of motion, can be evaluated on the fly. If the resonant frequencies were known, e.g., from experiment, it would be enough to propagate only a few trajectories in order to make qualitative assignment of the spectral features.

Note Added in Proof. A Molecular Dynamics calculation similar to the one reported here has just appeared. Sauer, J.; Döbler, J. *ChemPhysChem* **2005**, *6*, 1706.

Acknowledgment. We thank the National Science Foundation (NSF CHE-0446527) for funding this project.

References and Notes

(1) Zundel, G. In *The Hydrogen Bond: Recent Developments in Theory and Experiment*; Schuster, P., Zundel, G., Sandorfy, C., Eds.; North-Holland: Amsterdam, 1976; Vol. 2, p 683.
(2) Giruere, P. A.; Turrel, S. *Can. J. Chem.* **1976**, *54*, 3477.
(3) Librovich, N. B.; Sakun, V. P.; Sokolov, N. D. *Chem. Phys.* **1979**, *39*, 351.
(4) Atkins, P. W. *Physical Chemistry*; Freeman: New York, 1994.
(5) Nagler, J. F. In *Proton Transfer in Hydrogen Bonded Systems*; Bountis, T., Ed.; Plenum: New York, 1992; p 17.
(6) Mitchell, P. *Science* **1979**, *206*, 148.
(7) Marx, D.; Tuckerman, M. E.; Hutter, J.; Parrinello, M. *Nature* **1999**, *397*, 601.
(8) Tuckerman, M. E.; Marx, D.; Parrinello, M. *Nature* **2002**, *417*, 925.
(9) Fridgen, T. D.; McMahon, T. B.; MacAleese, L.; Lemaire, J.; Maitre, P. *J. Phys. Chem. A* **2004**, *108*, 9008.
(10) Asmis, K. R.; Pivonka, N. L.; Santambrogio, G.; Brummer, M.; Kaposta, C.; Neumark, D. M.; Woste, L. *Science* **2003**, *299*, 1375.
(11) Mella, M.; Clary, D. C. *J. Chem. Phys.* **2003**, *119*, 10048.
(12) Dai, J.; Bacic, Z.; Huang, X.; Carter, S.; Bowman, J. M. *J. Chem. Phys.* **2003**, *119*, 6571.
(13) Huang, X.; Braams, B. J.; Carter, S.; Bowman, J. M. *J. Am. Chem. Soc.* **2004**, *126*, 5042.
(14) Lobaugh, J.; Voth, G. A. *J. Chem. Phys.* **1996**, *104*, 2056.
(15) Valeev, E. F.; Schaefer, H. F. *J. Chem. Phys.* **1998**, *108*, 7197.
(16) Xantheas, S. S. *J. Am. Chem. Soc.* **1995**, *117*, 10373.
(17) Perez del Valle, C.; Novoa, J. J. *Chem. Phys. Lett.* **1997**, *269*, 401.
(18) Samson, C. C. M.; Klopper, W. *J. Mol. Struct. THEOCHEM* **2002**, *586*, 201.
(19) Yeh, L. I.; Okumura, M.; Meyers, J. D.; Price, J. M.; Lee, Y. T. *J. Chem. Phys.* **1989**, *91*, 7319.
(20) Price, E. A.; Robertson, W. H.; Diken, E. G.; Weddle, G. H.; Johnson, M. A. *Chem. Phys. Lett.* **2002**, *366*, 412.
(21) Lami, A.; Villani, G. *Chem. Phys. Lett.* **1995**, *238*, 137.
(22) Lami, A.; Villani, G. *J. Mol. Struct. THEOCHEM* **1995**, *330*, 307.
(23) Huang, X.; Cho, H. M.; Carter, S.; Ojamae, L.; Bowman, J. M.; Singer, S. J. *J. Phys. Chem. A* **2003**, *107*, 7142.
(24) Robertson, W. H.; Diken, E. G.; Price, E. A.; Shin, J. W.; Johnson, M. A. *Science* **2003**, *299*, 1367.
(25) Termath, V.; Sauer, J. *Mol. Phys.* **1997**, *91*, 963.
(26) Vener, M. V.; Kuhn, O.; Sauer, J. *J. Chem. Phys.* **2001**, *114*, 240.
(27) Huang, X.; Braams, B. J.; Bowman, J. M. *J. Chem. Phys.* **2005**, *122*, 044308.
(28) McCoy, A. B. Huang, X.; Carter, S.; Landerweer, M. Y.; Bowman, J. M. *J. Chem. Phys.* **2005**, *122*, 061101.
(29) Vener, M. V.; Sauer, J. *Chem. Phys. Lett.* **1999**, *312*, 591.
(30) Wei, D.; Salahub, D. R. *J. Chem. Phys.* **1997**, *106*, 6086.
(31) Cheng, H.-P.; Krause, J. L. *J. Chem. Phys.* **1997**, *107*, 8461.
(32) Cheng, H.-P. *J. Phys. Chem. A* **1998**, *102*, 6201.
(33) Wales, D. J. *J. Chem. Phys.* **1999**, *110*, 10403.
(34) Headrick, J. M.; Bopp, J. C.; Johnson, M. A. *J. Chem. Phys.* **2004**, *121*, 11523.
(35) Diken, E. G.; Headrick, J. M.; Roscioli, J. R.; Bopp, J. C.; Johnson, M. A.; McCoy, A. B. *J. Phys. Chem. A* **2005**, *109*, 1487.
(36) Hammer, I. N.; Diken, E. G.; Roscioli, J. R.; Johnson, M. A.; Myshakin, E. M.; Jordan, K. D.; McCoy, A. B.; Huang, X.; Bowman, J. M.; Carter, S. *J. Chem. Phys.* **2005**, *122*, 244301.
(37) Bowman, J. M.; Zhang, X.; Brown, A. *J. Chem. Phys.* **2003**, *119*, 646.
(38) Kaledin, M.; Brown, A.; Kaledin, A. L.; Bowman, J. M. *J. Chem. Phys.* **2004**, *121*, 5646.
(39) Kaledin, M.; Kaledin, A. L.; Brown, A.; Bowman, J. M. In *Normal-Mode Analysis: Theory and Applications to Biological and Chemical Systems*; Cui, Q., Bahar, I., Eds.; CRC Press: Boca Raton, FL, 2005.
(40) Berens, P. H.; Wilson, K. R. *J. Chem. Phys.* **1981**, *74*, 4872.
(41) Metropolis, N.; Rosenbluth, A. W.; Rosenbluth, M. N.; Teller, A. H.; Teller, E. *J. Chem. Phys.* **1953**, *21*, 1087.
(42) Noid, D. W.; Koszykowski, M. L.; Marcus, R. A. *J. Chem. Phys.* **1977**, *67*, 404.
(43) Wales, D. J. *J. Chem. Phys.* **1999**, *110*, 10403.
(44) Brooks, B. R.; Janezic, D.; Karplus, M. *J. Comput. Chem.* **1995**, *12*, 1522.